CHALMERS

Isotope Effects in Evaporation from Small Water Clusters

Kaveh Najafian

Department of Fundamental Physics
Chalmers University of Technology
Gothenburg, Sweden 2014

Abstract

The statistical decay of light and heavy water from ionic water clusters of 4 - 22 molecules was measured in vacuum. The rate constants were found to be increasingly favored towards evaporation of light water compared to the heavier isotopologues, with increasing cluster size. Calculations of the partition functions of H_2O, HDO and D_2O are presented and used to investigate the origin of the observed rate constants. Competing effects were found between the higher partition function and the higher dissociation energy of the heavier isotopologues, leading to an overall favored H_2O evaporation. The rate constants are found to depend exponentially on the deuterium concentration in the cluster, which may be explained by a second order indirect interaction between deuterium and neighboring hydrogen bonds in the cluster.

Acknowledgements

I would like to express my love for my family and friends, without whom I have nothing of value. I would also like to thank the collaborators of this thesis for including me and making the experiment possible. In particular I owe a great thanks to Klavs Hansen for investing his time in me for more than two years with impeccable patience and enthusiasm.

Kaveh Najafian, Gothenburg 14/03/14

Contents

1

Introduction

Water is one of the most abundant molecules in the universe. It has been observed 12 billion light years away[1] as well as in the interstellar medium and on many planets in our solar system. Apart from the importance of water in astrochemical, biological and atmospheric processes it is also interesting because of its many unique properties. These include a high surface tension, large heat capacity and a lower density in the solid phase compared to the liquid. It is therefore no surprise the extent to which water has been studied, both macroscopically and microscopically, over a long period of time.

Here on earth, water clusters play an important role in atmospheric processes and in particular in climate modeling seeing as water vapor is the most abundant greenhouse gas. Most ionized water clusters are formed in the troposphere by collisions with cosmic rays, where they trigger cloud formation[2]. The study of clusters is also a means of understanding some of the interesting properties of water in bulk. Many characteristics of bulk water arise from the nature of the intermolecular hydrogen bond, and by studying clusters we can probe this bond on the smallest scales.

The exchange of one or more hydrogen in the molecule with a deuterium is a commonly used technique to probe some properties of the hydrogen bond. Studies on the isotope effects of water in bulk have found differences between light and heavy water in the melting point[3] as well as in the evaporation[4]. A recent study found the presence of broken bonds between molecules to be 50% more common for the hydrogen than the deuterium bonds in bulk water[5]. Calculations of the energy of the bond have found similar effects when substituting hydrogen for deuterium. The difference in evaporation and condensation is also used in paleothermometry to determine the temperature of a sample based on the heavy-water fraction. Observing these differences experimentally in the smallest clusters is often difficult and extensive studies are devoted instead to

calculating their geometrical structure and attributes.

The experiment that is presented in this thesis aims at studying some of the smallest protonated water clusters $(H_2O)_N H^+$, with $N = 4$ - 22. These are comparatively easy to produce and manipulate using electric fields. By substitution of hydrogen with deuterium we hope to measure the isotope effects in the spontaneous evaporation of molecules from the clusters. Using a mixture of heavy- and light-water in the source, we will observe the decay of different isotopologues at the same time, with the same energy distribution. This allows us to rule out several potential causes of the measured asymmetry between H_2O, HDO and D_2O.

The clusters are produced in an electrospray ionization source at atmospheric pressure. They enter into vacuum and are mass selected in a quadrupole filter. They can then evaporate freely for some time before we measure the decay products in a time-of-flight mass spectrometer. Each cluster size, N, and deuterium composition, $D = 0$ - $(2N+1)$, will be mass selected and the evaporation spectrum recorded. This way we will probe the decay by emission of all three molecules at the same time. The details of the experimental setup and procedure are found in Chapter 3. We will analyze the spectra with regard to the difference in evaporation between light and heavy water. The ratio of evaporation will depend on the number of deuterium in the clusters, and this is factored out to retrieve the relative decay rate constants of each isotopologue (Section 4.4). These are in turn analyzed using the theory of thermal decay and the calculations of the partition functions and temperatures in Chapter 2, to yield the difference in dissociation energies. The number of evaporated molecules will also be analyzed, as a function of cluster size and deuterium content (Section 4.2). Results and some immediate analysis and discussion is presented in Chapter 4. The thesis will end with some conclusions and comparison of our results with previous work, in Chapter 5.

The main contributions of this thesis are:

- The direct observation of isotope effects in the evaporation of H_2O, HDO and D_2O in water clusters of 4 - 22 molecules. This is expressed quantitatively as the relative rate-constants of each isotopologue. The ratio of rate-constants increases with cluster size up to $N = 10$ and remains nearly constant in larger clusters. In the larger clusters we find a significant difference in the evaporation, with an average ratio $1 : 0.55 : 0.43$ of the rate constants $k_{H_2O} : k_{HDO} : k_{D_2O}$. (Section 4.4)

- Calculation of the internal partition functions of H_2O, HDO and D_2O, that are needed to analyze the measured rate-constants. Lists of experimental energy-levels and their associated quantum numbers are used to calculate the canonical partition functions. The importance of nuclear spin statistics in the partition functions, and by extension the rate-constants, is verified. The ratio of $Z_{H_2O} : Z_{HDO} : Z_{D_2O}$ is calculated to be constant between 30 - 500 K, and amounts to $1 : 4.9 : 5.8$. (Section

2.2)

- Relating the observed rate-constants using the theory of thermal decay and the evaporative ensemble to a difference in dissociation energies. The difference is found to increase with cluster size, which (amongst other things) reflects the average number of hydrogen bonds in the cluster. In clusters $N = 9$ and larger the dissociation energy of HDO is 25.8 meV higher than for H_2O, the dissociation energy of D_2O is 31.0 meV higher than for H_2O and the dissociation energy of D_2O is 6.4 meV higher than for HDO. (Section 4.4)

- The direct observation that the heat capacity does not significantly depend on the number of deuterium in the cluster, by looking at the fraction of clusters that have decayed in the experimental time window. (Section 4.2.2)

- Relating the exponential deuterium dependence of rate constants to second order interaction effects that a deuterium has on neighboring hydrogen bonds. (Section 4.5)

2

Theory

In this chapter some of the theory and calculations that are needed to analyze the experiment are presented. The first part deals with the statistical unimolecular decay of particles where an expression for the rate constant will be derived. Section two of this chapter presents calculations of the internal partition functions of the free H_2O HDO and D_2O molecules. In Section 2.3 the results of the two previous sections are used to estimate the temperatures of clusters in the experiment. Most of the equations in this chapter are from the book "Statistical Physics of Nanoparticles in the Gas Phase" by K. Hansen [6] where more detailed derivations can be found.

2.1 Unimolecular decay rate constants

All thermodynamic systems tend to equilibrate to their surroundings. This means that a cluster that is excited above the ambient temperature will lose some energy to its surroundings by collisions or through emission of particles or radiation. Unlike the loss of fragments through direct detachment, e.g. when an atom absorbs a photon with the energy of the electron affinity to detach an electron, the equilibration to the environment is a statistical process in which the energy is dispersed throughout all the degrees of freedom in the cluster prior to decay.

Such a process can be described by the principle of detailed balance, as was first suggested by Weisskopf for the emission of small fragments from nuclei [7]. The principle states that in a statistical process with a stationary environment, the rate of moving from one state to another is equal to the rate of moving in the opposite direction. The rates can be defined as the rate constants k_{decay} and $k_{formation}$ in units of inverse time, times

the relative density of each state,

$$\frac{\rho_p(E)}{\rho_p(E)+\rho_r(E)}k_{formation} = \frac{\rho_r(E)}{\rho_p(E)+\rho_r(E)}k_{decay}. \tag{2.1}$$

Here $\rho_p(E)$ and $\rho_r(E)$ refer to the product and reactant level densities. As an analogy we can think of Eq. (2.1) as the statement that if you have a bee inside your house and the density of bees is higher around your house, opening the window is more likely to invite another bee in than it is letting the first one out. [1]

The level density $\rho(E)$ is a useful measure of the number of quantum states of a system at a given energy. It will re-appear many times in this thesis and therefore merits some closer inspection. In the form $\rho(E)dE$ it is the number of states in the interval dE. For simple systems of one or more independent harmonic oscillators this can be calculated exactly [8], whereas more complicated systems of oscillators coupling to rotations and electronic states will at best rely on approximations.

The level density is also used to define what we mean by the temperature of a microscopic cluster in vacuum. The usual thermodynamic notion of a canonical temperature involves the exchange of energy of our cluster with a heat bath that is sufficiently large that the temperature of the heat bath itself is not affected by the exchange. Temperature is then defined through the level density of the heat bath $\rho_h(E)$ via the Boltzmann factor,

$$e^{-\varepsilon_i \frac{d\ln\rho_h(E)}{dE}} = e^{-\frac{\varepsilon_i}{k_B T}}, \tag{2.2}$$

that gives the relative population of each state ε_i in the cluster. In this sense it may seem strange to talk of a temperature of our isolated clusters that cool through emission of particles and not through equilibration to the walls of the machine. Instead the microcanonical temperature of a cluster is used with the cluster itself acting as a heat bath.

$$\frac{d\ln\rho(E)}{dE} = \frac{1}{k_B T} \tag{2.3}$$

The level density is now that of the cluster itself. Although this definition is valid for a cluster of many degrees of freedom, it is important to stress that this is a different concept of temperature than the canonical temperature.

Returning to eq (2.1), the rate constant for attachment of an incoming particle to a cluster confined in a volume V takes the form,

$$k_{formation}(\varepsilon_t) = \frac{1}{V}\sigma(\varepsilon_t)v, \tag{2.4}$$

[1] It is an empirical observation of the author that bees fly in random directions according to a stochastic process, which is the assumption that is required for this analogy to be valid.

where $\sigma(\varepsilon_t)$ is the attachment cross-section, $v = \sqrt{2\varepsilon_t/m}$ is the velocity of the incoming particle and ε_t is the kinetic energy of the particle. m refers to the reduced mass of the cluster and incoming particle. Thus we can re-write equation 2.1 as,

$$k_{decay}(E, \varepsilon_t) = \frac{1}{V}\sigma(\varepsilon_t)v\frac{\rho_p(E)}{\rho_r(E)}, \tag{2.5}$$

where ε_t now takes on the role of kinetic energy of the emitted fragment.

The product level density $\rho_p(E)$ can be evaluated as the convolution of the level density of the daughter cluster ρ_d with the level density of translations, $\rho_f(\varepsilon_t)$, and the internal level density of the evaporated fragment $\rho_f(\varepsilon_f)$,

$$\rho_p(E) = \int_0^E \rho_t(\varepsilon_t)\rho_f(\varepsilon_f)\rho_d(E - E_a - \varepsilon_t - \varepsilon_f)d\varepsilon_t d\varepsilon_f. \tag{2.6}$$

E_a is the dissociation energy of the molecule and ε_t and ε_f correspond to the energy carried away by the molecule as kinetic and internal energy.

The number of translational quantum states in the interval $d\varepsilon_t$ of the fragment emitted into volume V is,

$$\rho_t(\varepsilon_t)d\varepsilon_t = 4\pi\sqrt{2}\frac{Vm^{3/2}}{h^3}\varepsilon_t^{1/2}d\varepsilon_t. \tag{2.7}$$

We will insert this expression for ρ_t into Eq. (2.5) and integrate over the kinetic energy.

$$k_{decay}(E) = \int_0^E \frac{m}{\pi^2\hbar^3}\sigma(\epsilon_t)\epsilon_t\frac{\rho_f(\varepsilon_f)\rho_d(E - E_a - \varepsilon_t - \varepsilon_f)}{\rho_r(E)}d\epsilon, \tag{2.8}$$

Asuming the kinetic energy of the fragment is small compared to the internal energy of the daughter cluster, $E_d = E - E_a - \varepsilon_f - \varepsilon_t$, we can expand $\rho_d(E_d)$ around $E_\alpha = E - E_a - \varepsilon_f$ to easier evaluate this integral. The level density is a strongly varying function of energy and a better approximation in this case is to expand the logarithm and re-exponentiate to obtain,

$$\rho_d(E_\alpha - \varepsilon_t) = \exp\left(\ln\left[\rho_d(E_\alpha - \varepsilon_t)\right]\right) \tag{2.9}$$

$$\approx \exp\left(\ln\left[\rho_d(E_\alpha)\right] - \frac{\partial \ln \rho_d(E_\alpha - \varepsilon_t)}{\partial \varepsilon_t}\varepsilon_t\right) \tag{2.10}$$

$$= \rho_d(E_\alpha)e^{-\varepsilon_t\frac{\partial \ln \rho_d(E_\alpha - \varepsilon_t)}{\partial \varepsilon_t}} \tag{2.11}$$

$$= \rho_d(E_\alpha)e^{-\varepsilon_t/k_B T_d}, \tag{2.12}$$

where the definition of the microcanonical temperature was used in the last equality. The logarithmic derivative is evaluated at E_d which corresponds to the daughter temperature T_d. This approximation is a neat trick to simplify many expressions involving the level

density that will appear in this thesis. The integral in Eq. (2.8) is evaluated by first noting that[2],

$$\int_0^E \varepsilon_t e^{-\frac{\varepsilon_t}{k_B T_d}} d\varepsilon_t \approx (k_B T_d)^2 \int_0^\infty \frac{\varepsilon_t}{k_B T_d} e^{-\frac{\varepsilon_t}{k_B T_d}} d\left(\frac{\varepsilon_t}{k_B T_d}\right) = (k_b T_d)^2. \tag{2.13}$$

The rate constant is now close to its final form,

$$k_{decay}(E) = \frac{m}{\pi^2 \hbar^3} \langle\sigma\rangle (k_B T_d)^2 \frac{\rho_f(\varepsilon_f)\rho_d(E - E_a - \varepsilon_f)}{\rho_r(E)}, \tag{2.14}$$

with $\langle\sigma\rangle$ representing the cross-section averaged over kinetic energy,

$$\langle\sigma\rangle = \frac{\int_0^E \sigma(\varepsilon_t)\varepsilon_t e^{-\varepsilon_t/k_B T_d} d\varepsilon_t}{\int_0^E \varepsilon_t e^{-\varepsilon_t/k_B T_d} d\varepsilon_t}. \tag{2.15}$$

We can treat the internal energy of the evaporated fragment ε_f in a similar fashion if we assume this is also small compared to E_d. As we have seen from Eq. (2.12) the expansion of $\rho_d(E - E_a - \varepsilon_f)$ around $E - E_a$ will produce $\rho_d(E - E_a)\exp(-\varepsilon_f/k_B T_d)$. Unlike the translational level density we don't know the explicit form of $\rho_f(\varepsilon_f)$. Instead we note that the integral of the level density times a Boltzmann factor produces the canonical partition function Z_{int},

$$Z_{int} = \int_0^\infty \rho_f(\varepsilon_f) e^{\frac{-\varepsilon_f}{k_B T_d}} d\varepsilon_f \tag{2.16}$$

The internal partition function is calculated for H_2O, HDO and D_2O in section 2.2. Putting the results together we have now obtained a useful expression for the rate constant for evaporation of molecules from a cluster.

$$k_{decay}(E) = \frac{m}{\pi^2 \hbar^3} \langle\sigma\rangle (k_B T_d)^2 Z_{int} \frac{\rho_d(E - E_a)}{\rho_p(E)}, \tag{2.17}$$

where the subscripts d and p now refer to the daughter and parent clusters. The only assumption that was made in this derivation is that the cluster retains most of its internal energy after the decay. This expression will be helpful to understand the origin of the different rate constants in Chapter 4. The following two sections of this chapter are devoted to finding the partition functions Z_{int} and daughter temperatures T_d that appear in this expression.

2.2 Partition functions of H_2O, HDO and D_2O

The internal partition function that appears in Eq. (2.17) was computed for all three water species using the canonical expression,

$$Z_{int} = \sum_i (2J_i + 1) g_i \exp\left(-\frac{E_i}{k_B T}\right). \tag{2.18}$$

where i runs over all rotational states of the system. g_i and E_i are the degeneracies and energy levels of each state. We can assume that the water molecules are in their vibrational and electronic ground states. The first excited vibrational state of H_2O has an energy of 0.18 eV, and with a temperature of $\approx$ 150 K the contribution from the Boltzmann factor in Eq. (2.18) is on the order of 10^{-7}. The temperature T of the water molecule is defined using the parent cluster as the heat bath, assuming that the fragment is so small as not to carry away a significant amount of the energy or the degrees of freedom from the cluster. The microcanonical temperature of the cluster is evaluated at the energy $E_d = E - E_a - \varepsilon_f$, where ε_f is the energy carried away by the fragment. This corresponds to the daughter temperature. In this way we can treat quantities like the partition function of a free water molecule canonically, as having a temperature equal to the microcanonical temperature of the daughter cluster.

The spin-statistical degeneracy g_i is analyzed in the following manner. The Pauli principle leads to constraints on the parity of the molecular wavefunction, Ψ_{tot}, to be antisymmetric under interchange of identical fermions $P(\Psi_{tot}) = -\Psi_{tot}$. This applies to interchange of the hydrogen in H_2O about the symmetry axis. Bosons on the other hand, such as the deuterium nuclei in D_2O, must produce a total molecular wavefunction that is symmetric under parity $P(\Psi_{tot}) = +\Psi_{tot}$. The parity of the combined molecular wavefunction is a combination of the rotational (Ψ_{rot}), nuclear (Ψ_{nuc}), vibrational (Ψ_{vib}) and electronic (Ψ_{el}) parities.

$$P(\Psi_{tot}) = P(\Psi_{rot})P(\Psi_{nuc})P(\Psi_{vib})P(\Psi_{el}) \tag{2.19}$$

The vibrational and electronic ground state is symmetric under exchange of nuclei so only rotational and nuclear parities need to be considered. Therefore if the rotational wave-function of H_2O is of even parity $P(\Psi_{rot}) = +\Psi_{rot}$, the nuclear wave-function must be of odd parity $P(\Psi_{nuc}) = -\Psi_{nuc}$ corresponding to the antisymmetric singlet state of two spin 1/2 particles,

$$|\Psi^-_{nuc}\rangle = \frac{1}{\sqrt{2}}(|\uparrow\downarrow\rangle - |\downarrow\uparrow\rangle). \tag{2.20}$$

The antisymmetric rotational wave function $P(\Psi_{rot}) = -\Psi_{rot}$ on the other hand leads to constraints on the nuclear wave-function to be symmetric $P(\Psi_{nuc}) = \Psi_{nuc}$, which is the 3-fold degenerate triplet state. The symmetric and antisymmetric spin degeneracy of H_2O and D_2O is 3:1 and 6:3 correspondingly. There are no parity constraints on HDO and all states have a degeneracy corresponding to the number of combinations of the combined hydrogen and deuterium system. A single spin 1/2 particle has two possible projections and a spin 1 has three and thus all states are 6-fold degenerate. We will now move on to find the parity and energy levels of the rotational states of an asymmetric top molecule.

The asymmetric-top rigid-rotor Hamiltonian is given by

$$\hat{H}_R = A\hat{J}_a^2 + B\hat{J}_b^2 + C\hat{J}_c^2, \tag{2.21}$$

where A, B, C are the rotational constants, $A \equiv \hbar^2/(2I_A)$, with axes defined such that $I_A < I_B < I_C$. They are listed for the three water isotopes in table 2.1.

	H_2O	HDO	D_2O
I_A (10^{-40}g cm^2)	1.0220	1.2092	1.8384
I_B (10^{-40}g cm^2)	1.9187	3.0654	3.8340
I_C (10^{-40}g cm^2)	2.9376	4.2715	5.6698
$g_{symmetric}$	3	6	6
$g_{antisymmetric}$	1	6	3

Table 2.1: Moments of inertia and spin degeneracies of the three different water isotopes from [9].

The asymmetric top wavefunction can be approximated as a combination of the prolate ($I_A < I_B = I_C$) and oblate ($I_A = I_B < I_C$) symmetric-top wavefunctions. For a symmetric-top molecule the rotational quantum number J and the projection of J on the top axis K_A (K_C) of the prolate (oblate) symmetric top is enough to determine the rotational energy-levels. The wavefunction of the symmetric top rigid rotors are linear combinations of spherical harmonics $Y_{J,M}(\theta, \phi)$. Under a parity transformation $(\theta, \phi) \to (\pi - \theta, \phi + \pi)$ we have,

$$Y_{J,M}(\theta, \phi) \to Y_{J,M}(\pi - \theta, \phi + \pi) = (-1)^J Y_{J,M}(\theta, \phi), \tag{2.22}$$

where M is the quantum number specifying the orientation of the angular momentum in the laboratory reference frame and gives rise to the $(2J+1)$ degeneracy in Eq. (2.18). Thus the parity of the rotational wavefunction is given by $(-1)^J$.

The symmetric-top eigenfunctions $|JK_AM\rangle$ and $|JK_CM\rangle$ for the prolate and oblate rotors, form a complete basis for the asymmetric top hamiltonian,

$$|J\tau M\rangle = \sum_i c_{\tau i} |JK_iM\rangle \tag{2.23}$$

where $\tau = K_A - K_C$, is an index for each of the (internal) $2J + 1$ angular momentum projections. $K_A = 0$ represents the limiting case of the oblate symmetric top state and $K_C = 0$ corresponds to the projection of J entirely in the prolate symmetric top state K_A. In total $K_A + K_C$ amounts to J or $J + 1$ and the parity of the $|J\tau M\rangle$ level is therefore $(-1)^\tau$ [10].

The asymmetric top hamiltonian is only analytically soluble up to $J = 3$, and for higher rotational levels Eq. (2.21) must be diagonalized numerically. Using lists [11] [12] that combine the numerical approach with spectroscopic data, we obtain the energy

levels and associated quantum numbers (J, K_A, K_C) that are needed to evaluate Eq. 2.18. To illustrate how the partition function is calculated the ten lowest rotational energy levels and the parameters needed are listen in Table 2.2.

E_i [cm^{-1}]	J K_a K_c (parity)	g_i (parity)	Z' ($100K$)
0	0 0 0 (+)	6 (+)	6.00
12.1170	1 0 1 (-)	3 (-)	13.56
20.2592	1 1 1 (+)	6 (+)	27.01
22.6843	1 1 0 (-)	3 (-)	33.50
35.8782	2 0 2 (+)	6 (+)	51.41
42.0693	2 1 2 (-)	3 (-)	59.59
49.3396	2 1 1 (+)	6 (+)	74.35
73.6763	2 2 1 (-)	3 (-)	79.54
74.1422	2 2 0 (+)	6 (+)	89.87
70.4475	3 0 3 (-)	3 (-)	97.49

Table 2.2: The parameters used to calculate the partition function of D_2O using Eq. (2.18). The columns are from left to right: Energy of the rotational state, the quantum numbers associated with the state and the spin degeneracy factor g_i from the condition that the combined nuclear and rotational wavefunction must be symmetric under parity. The last column is the calculated partition function at 100K including the given and lower energy levels.

The partition functions calculated using all the available energy levels in [11] and [12] are plotted in Figure 2.1.

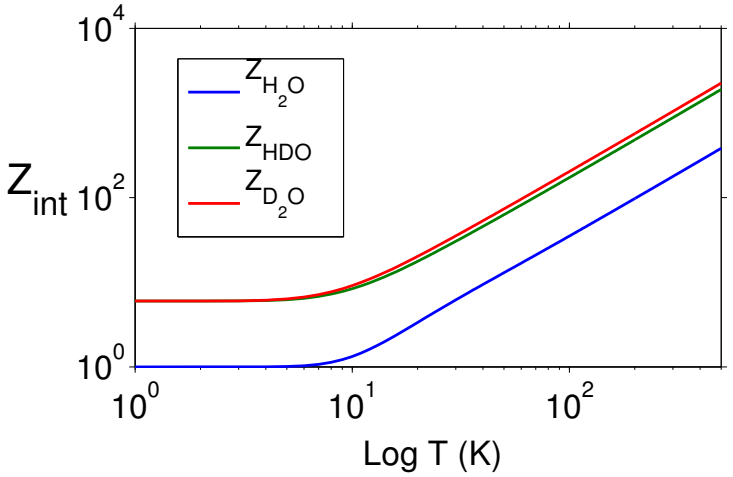

Figure 2.1: Internal partition functions for H_2O, HDO and D_2O, ranging from 0-500 K

Calculation of the partition functions of different water isotopes are the first result of this thesis, and in the next section they will be used to estimate the temperature of the clusters. In section 4.4 we will need the ratio of partition functions and these are plotted in figure 2.2. The ratio of $Z_{H_2O} : Z_{HDO} : Z_{D_2O}$ (henceforth $Z_0 : Z_1 : Z_2$) is fairly constant in the temperature range $30 - 500$ K and amounts to $1 : 4.9 : 5.8$. It is noteworthy that at a significant contribution to the difference is the nuclear spin statistics of different isotopes, and not only their moment of inertia. This is clearly seen in the ratio of Z_2/Z_1 which is close to unity.

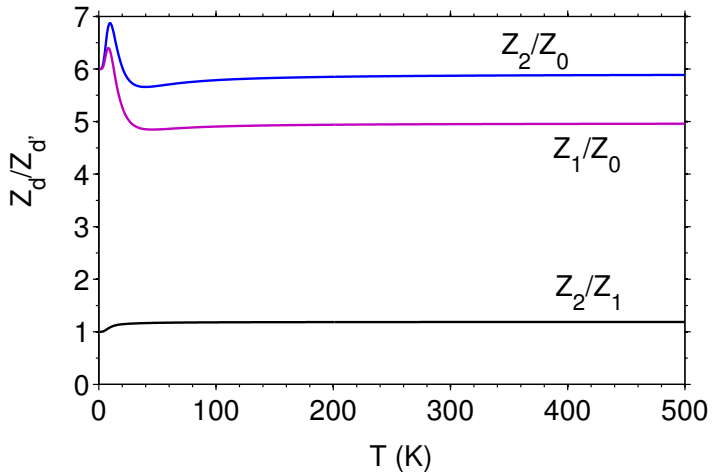

Figure 2.2: Ratios of the internal partition functions for H_2O, HDO and D_2O, from 0-500 K

2.3 Temperature estimates

In order to compare the derived rate constant in Eq. (2.17) with experimental data we need to get an idea of the microcanonical temperature of the cluster. Since we are unable to observe the decays that happen immediately after creation in the source, the hottest clusters will not be seen in the experiment. There is a maximum temperature $T_{max,N}$, depending on the dissociation energy $E_{a,N}$, above which the cluster will have already decayed before the experimental time window. The added subscript N now indicates that the maximum temperature and dissociation energy depends on the cluster size. We can find $T_{max,N}$ by writing the rate constant in the Arrhenius form

$$k(T) = \omega e^{-E_a/k_B T} \tag{2.24}$$

where we identify ω as the pre-factor to the ratio of level densities in Eq. (2.17),

$$\omega_N = \frac{m_N}{\pi^2\hbar^3}\langle\sigma_N\rangle(k_B T_N)^2 Z_{int}(T_N). \tag{2.25}$$

In the absence of other cooling channels (radiative, electronic emission etc.) the highest temperature of the clusters will obey the condition,

$$\omega e^{-E_{a,N}/k_B T} \approx \frac{1}{t_0} \tag{2.26}$$

$$\Rightarrow T = \frac{E_{a,N}}{k_B \ln(\omega t_0)} \tag{2.27}$$

The decay time t_0 is the time from entry into vacuum to after mass selection which corresponds to the earliest decay we can measure. The temperature T is an average between the parent and daughter temperature of the clusters, so to retrieve the maximum daughter temperature $T_{max,N}$ we will subtract half the dissociation energy from the internal energy of the cluster,

$$T_{max} = \frac{E_{a,N}}{k_B \ln(\omega t_0)} - \frac{E_{a,N}}{2C_N}. \tag{2.28}$$

C_N is the cluster size dependent heat capacity that has been reported previously for protonated water clusters $(H_2O)_N H^+$ in [13]. The clusters are all accelerated to the kinetic energy of 1eV and the flight path from creation to the first observable decays is 0.245m long. This means that $t_0 = 154\mu$s, for $N = 4$, which scales with $\sqrt{m}$ for the bigger clusters. ω will be estimated below in order to obtain the temperatures.

Since the frequency factor is itself a function of temperature, $\omega = \omega(T)$, the process of calculating the temperature and recalculating ω at this new temperature will be iterated until the temperature converges to a fixed value. In the calculation of ω_N the cross-section for attachment of a molecule to a cluster will be assumed to be the geometrical cross-section $\langle\sigma\rangle = \sigma_N$. For two spherical bodies of radii r_N and r_1 it takes the form,

$$\sigma_N = \pi(r_{N-1} + r_1)^2 = \pi r_1^2((N-1)^{1/3} + 1)^2 \approx \pi r_1^2 N^{2/3}, \tag{2.29}$$

where we have assumed that the radius r_N scales with $N^{1/3}$. As the spherical radius of a free water molecule the value $r = 2$ Å is used [14]. Table 2.3 shows the calculated ω_N and maximum daughter temperature of different cluster sizes as well as some parameters used in the calculation. Note that since ω_N enters into the logarithm, an error of factor 2 alters the value of T_{max} a few percent at most.

N	$Z_{int}(T_{max})$	ω_N [$\times 10^{17} s^{-1}$]	$E_{a,N}$ [eV]	$T_{max,N}[K]$
4	3	0.0003	0.685	26
5	15	0.0232	0.379	42
6	21	0.0556	0.374	66
7	30	0.1545	0.425	89
8	39	0.3151	0.466	108
9	47	0.5351	0.496	122
10	53	0.7648	0.513	133
11	56	0.9337	0.512	138
12	55	0.9708	0.490	137
13	56	1.0659	0.484	138
14	56	1.1200	0.472	138
20	59	1.6510	0.459	143
21	58	1.6686	0.452	142
22	49	1.1547	0.393	126

Table 2.3: The maximum temperature for each cluster size and the parameters used to calculate it using Eq. (2.28). The columns are from left to right: Cluster size, internal partition function, frequency factor ω, dissociation energies and maximum daughter temperature.

The temperature in Eq. (2.27) corresponds to an upper cutoff between the parent and daughter internal energy distribution of the clusters,

$$E_{max,N} = C_V \frac{E_{a,N}}{k_B \ln(\omega t)}. \tag{2.30}$$

The differential of this cutoff energy with respect to time will yield the decrease in maximum energy with time. After multiplication by the energy distribution $g(E)$ we obtain the decay rate R, i.e. the change in population over time,

$$R = g(E) \frac{C_V E_{a,N}}{k_B \ln^2(\omega t) t}. \tag{2.31}$$

We see that the number of decays over time is directly proportional to the heat capacity of the cluster. This observation will be useful when analyzing the metastable decay in section 4.2. We also see that the rate is proportional to the dissociation energy. This may be counter-intuitive since it suggests that the a higher dissociation energy will lead to more decays.

3

Experiment

The experiment was performed in collaboration with Mauritz Ryding and Einar Uggerud from the Department of Chemistry at Oslo University, Bertil Dynefors from the Department of Physics at Chalmers University of Technology and Klavs Hansen from the Department of Physics at the University of Gothenburg. The instrument used was a modified Q-Tof 2 mass spectrometer from Waters Corporation, UK. A schematic overview of the different regions of the instrument is shown in Figure 3.1.

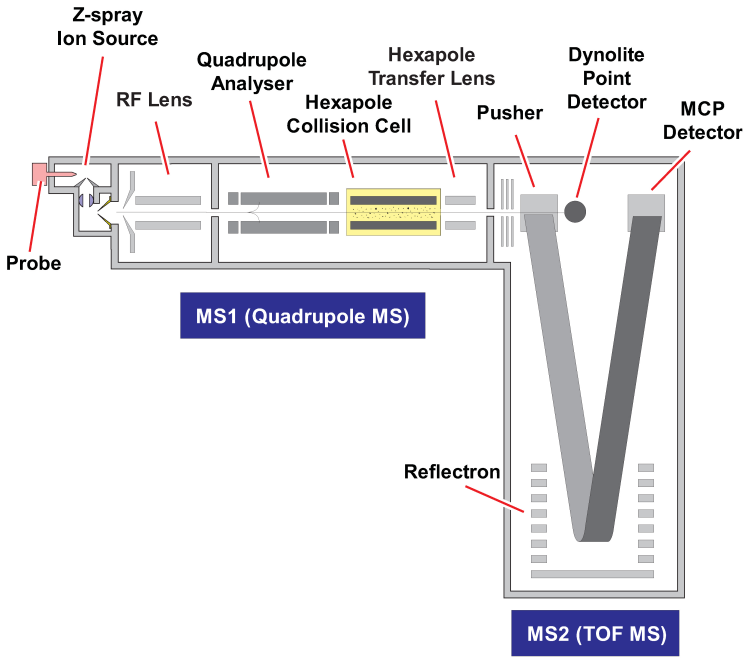

Figure 3.1: Schematic overview of the Q-Tof 2. © Waters Corporation. Used with permission.

The clusters are produced in an electrospray ion source at atmospheric pressure, and enter the vacuum part of the instrument through differentially pumped chambers. A specific cluster size and composition can be selected in the linear quadrupole filter. The clusters can then decay freely for some time before they reach the Time-Of-Flight mass-spectrometer (TOF MS), where the mass to charge ratio m/q of incoming ions are detected. Some sections of the instrument relevant for the current experiment are detailed in Section 3.1. The experimental procedure is described in the Section 3.2 and the final part of this chapter, Section 3.3 will deal with data handling and data reduction. More details about the experimental setup and similar experiments are found in [15].

3.1 Q-tof II

3.1.1 Electrospray ionisation source

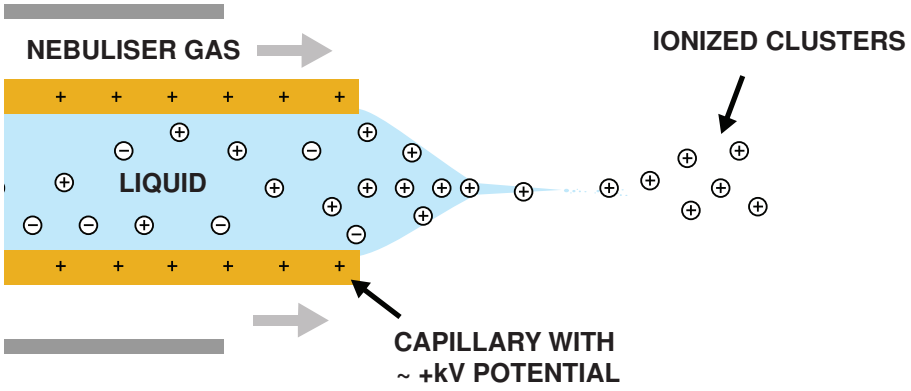

Figure 3.2: Schematic overview of the principles of electrospray ionization.

Electrospray ionization is a way of producing ions from a liquid that was first realized in the 1980's and subsequently awarded John Fenn with a Nobel Prize in Chemistry for its use on bio-molecules[16]. The liquid under study is fed through a needle that is held at a potential of a few keV. When this potential is strong enough the liquid will form a cone at the end of the needle (Taylor cone) and become ionized before finally escaping the needle as a jet of ionized droplets (See Fig. 3.2). A nebulizer gas will evaporate the droplets further and is used to decrease the size of the ionized clusters. Doubly charged water droplets will easily separate into singly charged species because of the added coulomb repulsion, and will not need to be considered in this experiment. The ions will then be accelerated by a fixed potential and led into vacuum through a series of differentially pumped chambers.

3.1.2 Quadrupole mass filter

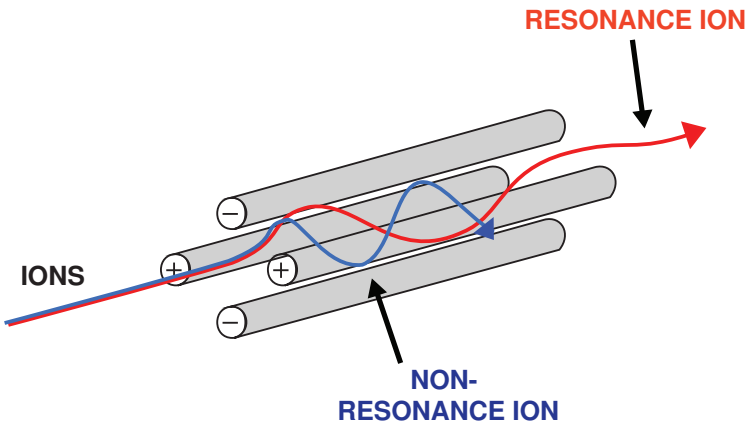

Figure 3.3: Schematic overview of the principles of a quadrupole mass filter.

The mass selection of a specific (or a range of) cluster sizes and compositions is achieved with a linear quadrupole mass filter. Four metal rods are arranged symmetrically around and parallel to the axis of the ion beam (See Figure 3.3). By applying a voltage over each opposing pair of rods Φ_+ and Φ_-, one can make the trajectories of ions with unwanted mass to charge ratios m/q unstable. The potentials can be described as,

$$\Phi_+ = +(U + V\cos\omega t),$$
$$\Phi_- = -(U + V\cos\omega t),$$

where $\omega = 2\pi\nu$ is a radio frequency alternating current with amplitude V and U is a static direct current. For a positive ion beam the positive DC potential of Φ_+ will repel the ions towards the center axis. Since the lower m/q is displaced more easily than the higher by the oscillating AC field, U and V and ν can be tuned so that all ions just below the desired ratio m/q will eventually hit the rod and be neutralized whereas the higher m/q will be less displaced by this field and survive through the filter. In a similar way Φ_- can be used to filter out the higher m/q ions. The DC potential is now attractive towards the rods but low m/q ions are kept from hitting them by the oscillating AC current. When combined these rods allow us to select a range of mass to charge ratios that will pass though the quadrupole. In the case where all ions have the same charge, this is effectively a mass filter that is used to select for a specific cluster size with a given number of deuterium in the cluster. Only the decays that happen between mass selection in the quadrupole and the TOF MS are detected in the experiment.

3.1.3 TOF MS

A time-of-flight mass-spectrometer is another way of determining the mass to charge ratio m/q of incoming ions. Ions of charge q exposed to a static field U will have a

potential energy $E_p = qU$. As they accelerate this potential energy will be converted into kinetic energy $E_k = \frac{1}{2}mv^2$. In the end the velocity will depend on the mass and charge as $v = \sqrt{2qU/m}$. The travel time to detection at a known distance d is then

$$t = \frac{d}{\sqrt{2U}} \cdot \sqrt{\frac{m}{q}}. \tag{3.1}$$

By detecting the time passed after acceleration by the potential U we can measure the ratio m/z.

This only works if the initial kinetic energy of the ions are the same, which is not always the case. Flight time uncertainties due to the small kinetic energy and spatial variations in the beam is minimized by using a reflectron. It consist of a constant electrostatic field and ions entering the region with higher energies will penetrate the field deeper before being reflected and therefore take slightly longer to reach the detector. This way the beam is focused so that all ions with the same m/q will reach the detector almost simultaneously irrespective of the initial spread in spatial and kinetic distribution. This allows for a very good m/z resolution.

The detector is a micro-channel plate that amplifies the signal as an electron multiplier when an incoming ion deposits some energy in one of the micro-channels.

3.2 Experimental procedure

A syringe and syringe pump was used to feed various fractions of pure H_2O and pure D_2O to the electrospray needle at $\sim 10\mu\text{Lmin}^{-1}$ in order to produce the desired cluster composition with good intensity. The ions were accelerated to $E_{lab} = 1\text{eV}$ of translational energy when entering vacuum and consequently the flight time through the different regions of the QTOF 2 will be determined by their mass, charge and the path lengths of each region. The flight times scale as $\sqrt{m}$ as shown in eq. 3.1.

The pressure in the quadrupole region varied between $8 - 10 \times 10^{-6}$mbar and the TOF pressure varied between $4 - 5 \times 10^{-7}$mbar for the duration of the experiment.

The TOF spectra were calibrated by putting pure H_2O in the syringe and comparing the calculated mass of $(H_2O)_{21}H^+$ (379.23 u) with the observed value (379.22 u). The quadrupole was then tuned to allow full intensity of this peak (mass ± 0.2 u). A second calibration point with $(H_2O)_4H^+$ (73.05 u) was used to cover a long range of cluster sizes accurately. Finally the calibration was tested with a $NaCl$-solution which showed good agreement with calculated masses.

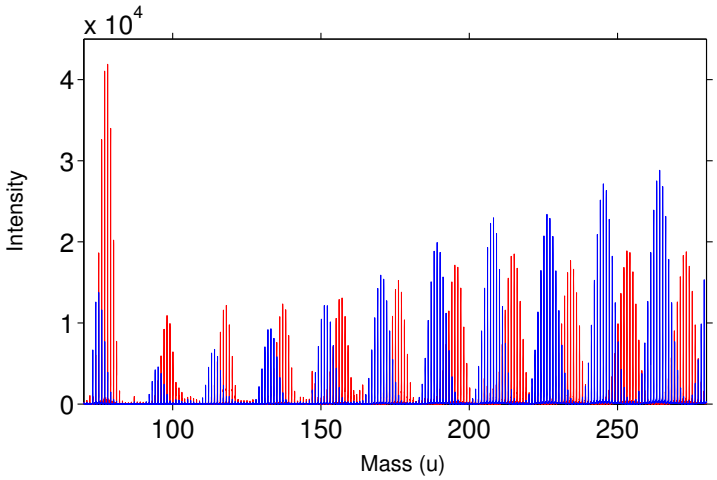

Figure 3.4: Two raw spectra with no mass selection showing masses 70-280 u, corresponding to cluster size N = 4-14. Blue spectrum was aquired with 10% D_2O in the source and red spectrum with 50% D_2O. No intensity normalization was done.

Figure 3.4 shows two raw spectra without mass selection, i.e. with the quadrupole off, using a 50/50 (red) and 90/10 (blue) ratio of H_2O/D_2O in the syringe. Each peak corresponds to a specific cluster size and composition $(H_2O)_N H^+$ with D hydrogen substituted for deuterium, ranging from $D = 0$ to $D = 2N + 1$. The shift in intensity towards higher deuterium content in the clusters as a function of the D_2O fraction in the source is clearly seen, and will be analyzed in Section 4.1.

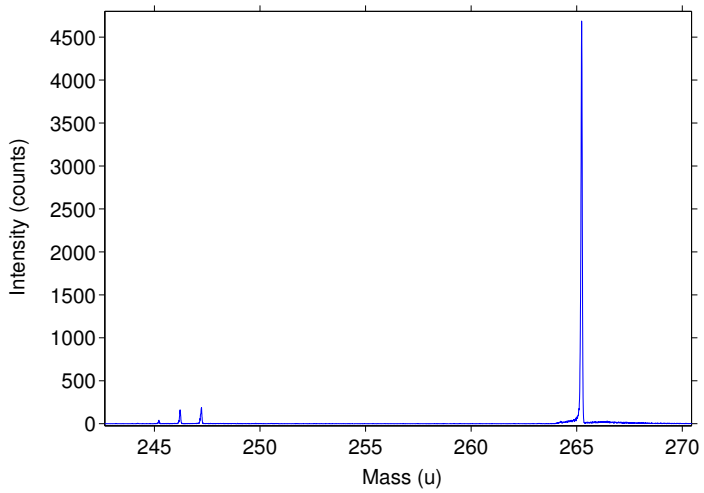

Figure 3.5: Raw spectrum with mass selection m = 265 u, corresponding to cluster size N = 14 D = 12. The three daughter-peaks correspond to loss of D_2O, HDO and H_2O from left to right.

Every possible composition of cluster sizes $N = 4$ to 14 and $N = 20$ to 22 was individually mass-selected in the quadrupole and the evaporation spectrum recorded. An example of an evaporation spectrum of $N = 14$, $D = 12$ is shown in figure 3.5. The large peak is the number of un-evaporated clusters and the three small peaks correspond to the number of clusters that have evaporated D_2O, HDO and H_2O from left to right. This way the relative weights of each decay channel is measured at the same time, under the same conditions.

The heavy- to light-water ratio in the source was tuned to give good intensity of the specific peak under study, typically around 200-300 counts/s in the parent peak. Each spectrum was recorded over 1-2 minutes to accumulate at least 2000 counts in the integrated daughter-peaks. Peaks of lower intensity were run longer. There is an overlap in mass between different D-compositions of two neighboring clusters, as can be seen in fig. 3.4. Extra care was taken with the D_2O fraction in the source to ensure that the right cluster size was being observed.

3.3 Data handling

Each evaporation-spectrum was imported into MATLAB. The instrument saves the accumulated mass spectrum from the buffer memory at given intervals (scans) and the counts in each mass channel was summed up over all scans of the spectrum. The parent- and daughter-peaks were integrated over their corresponding mass channels ± 0.1u. Daughter peaks that should not be observed, (e.g. corresponding to loss of H_2O in a heavy water-only cluster), ranged from $0 - 8\%$ of the branching ratios. These ”ghost peaks” were visible when the intensity of the parent cluster was below 30 counts/s and are assigned

to contaminations. The contaminations were subtracted in the following manner. HDO peaks were corrected by interpolating the HDO-loss, normalized to the total intensity,

$$I_{HDO}/(I_{parent} + I_{H_2O} + I_{HDO} + I_{D_2O}), \tag{3.2}$$

between the two cluster compositions corresponding to only hydrogen ($D = 0$), and only deuterium ($D = 2N + 1$), for each N. I_i refers to the integrated intensity of each peak. The intensity-normalized counts were then subtracted from each HDO peak in the given cluster size. Similarly for H_2O and D_2O there are two deuterium compositions with each cluster size, for which no evaporation should occur. An average over these two intensity-normalized counts was subtracted from all compositions. The correction of contaminations is easily illustrated by using the branching ratios,

$$B_d = \frac{I_d}{I_0 + I_1 + I_2}, \tag{3.3}$$

with $d = 0, 1, 2$ corresponding to H_2O, HDO and D_2O respectively. They are plotted with the original data (symbols) and corrected data (lines) for one cluster size in figure 3.6. The figure also shows the statistical uncertainty of the measured branching ratios. Black points indicate an evaporation spectrum that was reproduced on a different day, and shows the reproducibility of the experiment to be good.

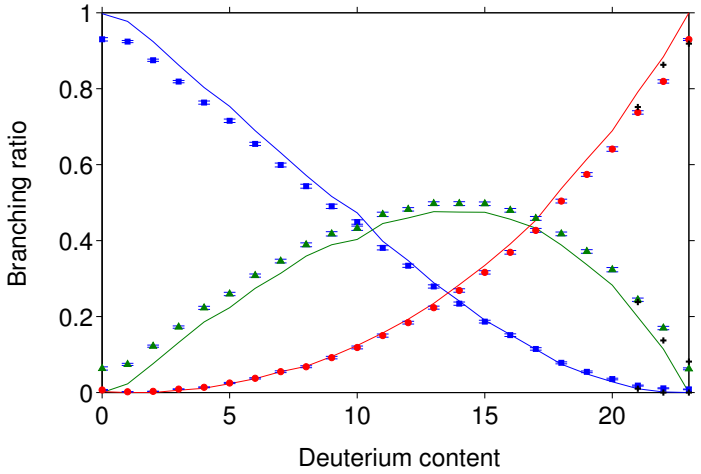

Figure 3.6: Branching ratios of H_2O, HDO and D_2O shown as squares, triangles and circles respectively, for cluster size $N = 11$. The lines are the corrected data as detailed in this section. Black crosses indicate a spectrum that has been measured twice to check reproducibility.

4

Results and Analysis

This chapter presents the analysis and results of the experiment, starting with the isotope distribution of the clusters in section 4.1, to see how the clusters are produced. The metastable decay fractions are presented in section 4.2, as a function of cluster size and deuterium content. Some observations are made regarding how the clusters are produced and their heat-capacities. Branching ratios are the relative weights of each decay-channel and they are presented in section 4.3, along with a comparison of the expected branching ratios if the rate constants were identical. The most significant result of this thesis is presented in 4.4, where we find the relative rate-constants as a function of cluster size and the difference in dissociation energies to explain the rate-constants. Finally in 4.5 we observe how the rate constants depend on the number of deuterium in the cluster.

4.1 Isotopic distribution

By using the full spectrum with no mass selection as seen in figure 3.4, we can analyze the distribution of isotopes reaching the TOF MS. These distributions correspond to a combination of what is produced in the source and the decay before the TOF. If the $2N+1$ sites in a cluster is occupied by D deuterium independently and at random with probability p of choosing deuterium for any site, we will have a binomial probability distribution of isotopes with each cluster size N.

$$B(D) = \binom{2N+1}{D} p^D (1-p)^{2N+1-D} \tag{4.1}$$

A χ^2 test for goodness of fit was employed to determine whether the observed distributions are binomial.

$$\chi^2 = \sum_{D=0}^{2N+1} \frac{(I_e(D) - I_f(D))^2}{\sigma_{I_e}^2}, \tag{4.2}$$

where $I_e(D)$ is the experimental integrated peak value and $I_f(D) = c \cdot B(D)$ is the expected value in the case of a binomial distribution. The uncertainty of the integrated peak is $\sigma_{I_e} = \sqrt{I_e}$ and the variance in the denominator is therefore $\sigma^2_{I_e} = I_e(D)$. The normalization factor c can be determined analytically by varying χ^2 with respect to c and finding the minimum value.

$$\frac{d\chi^2}{dc} = 0 \Longrightarrow \tag{4.3}$$

$$-2 \sum_{D=0}^{2N+1} \frac{1}{I_e(D)} \left[(I_e(D) - c \cdot B(D)) \cdot B(D) \right] = 0 \tag{4.4}$$

$$\Longrightarrow c = \frac{\sum_{D=0}^{2N+1} B(D)}{\sum_{D=0}^{2N+1} B(D)^2 / I_e(D)} \tag{4.5}$$

The probability p is determined numerically by varying p between $0-1$ in equation 4.2 and choosing the p that gives the smallest value of χ^2. Figure 4.1 shows two spectra with 50% and 80% D_2O in the source, fitted with binomial distributions according to this procedure.

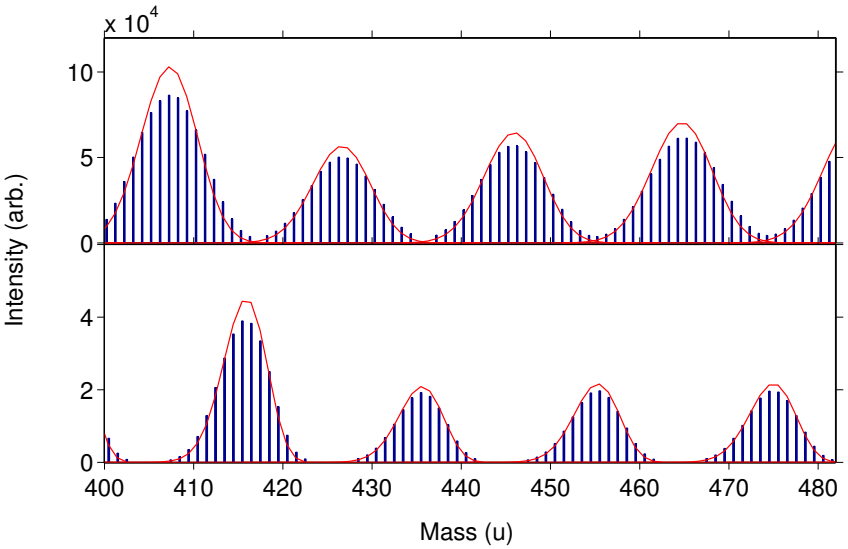

Figure 4.1: Spectra showing integrated peaks of $N = 21-24$ fitted with binomial distributions (solid line). Top spectrum acquired with 50% D_2O in the source and bottom spectrum acquired with 80% D_2O in the source.

With the χ^2 per degree of freedom we find the binomial distribution to give reasonable agreement with data with the exception of clusters $N = 3$ and $N = 4$. Clusters $N = 5$-26 give consistently good agreement although they tend to be wider than the binomial

distribution. Figure 4.2 shows the fitted value of p as a function of cluster size for different source D_2O fractions.

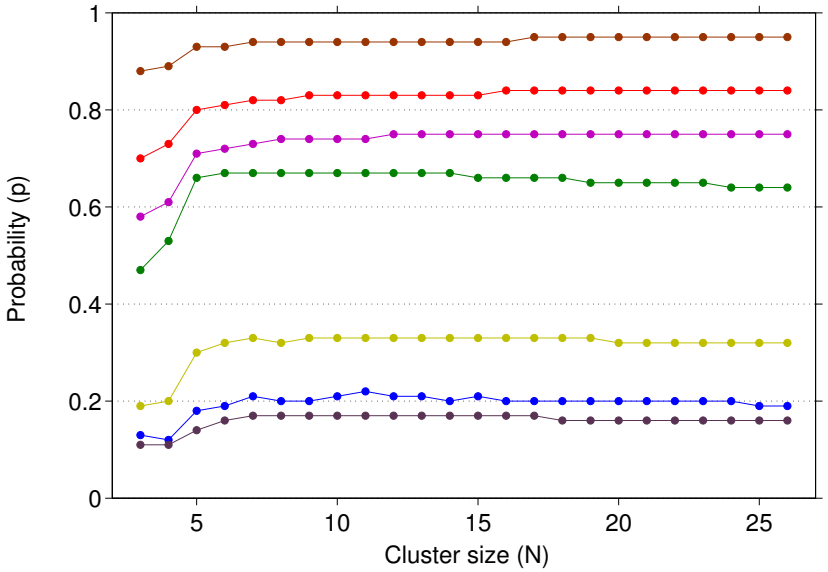

Figure 4.2: The fitted value of the deuterium fraction p according to the binomial fit as a function of cluster size N. From top to bottom the specta were acquired with 100%, 80%, 66%, 50%, 20%, 10% and 0% D_2O in the source respectively.

With the exception of the very smallest clusters, p is seen to be constant which is an indication of how the clusters are created before entering the TOF. If the clusters are created by repeated evaporation from larger clusters, p would decrease with increasing cluster size. The reason for this is that if the loss of hydrogen species is favored, more and more deuterium is left behind in smaller clusters. The fact that p is constant in figure 4.2 can therefore either mean that the rate-constants are not significantly different for loss of H_2O compared to D_2O, or that clusters do not decay much before detection.

We can estimate how many molecules are lost to evaporation before equilibrating to the vacuum temperature in the machine. With a heat capacity of $6k_B$ per molecule[13] the internal energy of the cluster with temperature T will be

$$E = N \cdot 6 \ k_B \cdot T \tag{4.6}$$

The clusters are created at room temperature ($E = N \cdot 0.16\text{eV}$) and assuming a vacuum temperature of roughly 100 K ($E = N \cdot 0.05\text{eV}$) we have a difference in internal energy of $\Delta E = N \cdot 0.11\text{eV}$. We will assume a constant heat capacity which is a good approximation for large clusters. With a dissociation energy of $\approx 0.45\text{eV}$ [17] the cluster will lose on average $N \cdot 0.11/0.45$ or $N/4$ molecules before reaching equilibrium temperature. From this we can conclude that all cluster sizes are produced in the source and do not

decay much before stabilizing. As an example cluster $N = 12$ will lose three molecules before stabilizing. Even with different decay rate-constants this will not significantly change the isotope distribution of smaller clusters which explains why the probability p is constant.

The average value of p as a function of the D_2O fraction in the source is plotted in figure 4.3. There is a shift towards higher deuterium content than in the source that may be explained by more evaporation of light water. It is also clear from the pure H_2O and pure D_2O spectra that there are contaminations in the machine of both light and heavy water.

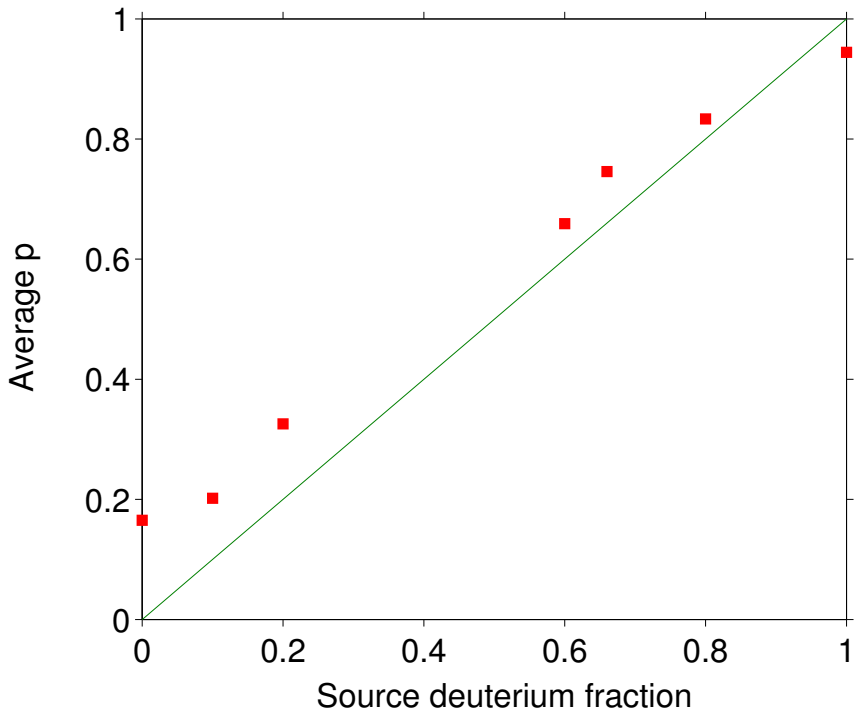

Figure 4.3: The fitted value of the deuterium probability p averaged over cluster sizes $N = 6$-26 as a function of the D_2O fraction in the source. The line is the expected curve in case there was a 1:1 relation between the deuterium fraction in the source and the observed probability.

4.2 Metastable fractions

The term ”metastable decay fractions” refers to the fraction of clusters that have undergone decay in the experimental time window. The fraction is defined as the ratio

between the number of evaporated clusters and the total intensity,

$$f_m = \frac{I_0 + I_1 + I_2}{I_0 + I_1 + I_2 + I_{parent}}. \tag{4.7}$$

This is analyzed as a function of cluster size in Section 4.2.1 and deuterium content in Section 4.2.2.

4.2.1 Evaporated fraction vs. cluster size

The evaporated fraction from cluster compositions with all three decay channels present, $D = 2$ - $(2N - 1)$, is plotted as a function of the cluster size N in figure 4.4.

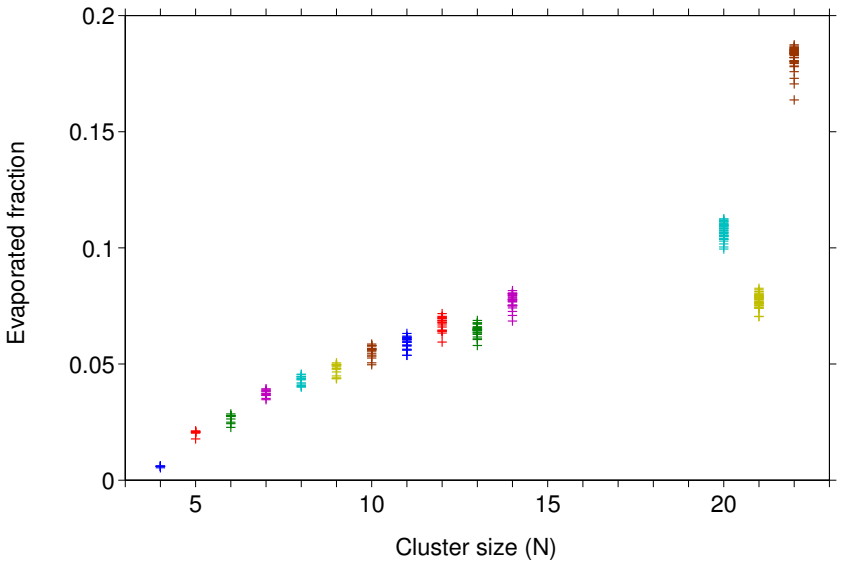

Figure 4.4: The fraction of evaporated water-molecules versus cluster size.

The cluster size dependence looks as expected with the evaporation increasing smoothly for larger clusters. This reflects the heat capacity and dissociation energies of the water-clusters. The heat capacities of protonated water clusters have been shown to be nearly linear in cluster size [13] with $C_{v,N} \approx 6(N-2) \cdot k_B$ and the decay rate was shown in Eq. 2.31 to be proportional to the heat capacity. If the dissociation energies $E_{a,N}$ were identical we would expect the evaporated fraction in figure 4.4 to be linear in N. The deviation from linearity seen is therefore attributed to a difference in dissociation energies from different cluster sizes. The anomaly around $N = 21$ is also apparent and has been attributed to a geometrical shell closing at this 'magic number', after which the dissociation energy is lower for clusters $N = 22$ and larger[17]. The smaller dissociation energy of $N = 22$ also results in the lower end of the energy distribution of the daughter

$N = 21$ to be shifted towards lower energies, which explains why this cluster evaporates less than the neighboring $N = 20$. As mentioned above, the dissociation energies and heat capacities of protonated light water clusters have been reported previously and will therefore not be treated in detail here.

4.2.2 Evaporated fraction vs. deuterium content

The evaporated fraction of molecules as a function of the relative deuterium content in the cluster is plotted in fig. 4.5. It is seen to be nearly constant within each cluster size. The fluctuations are not due to statistics and most likely reflect varying source conditions. From this figure we can conclude that the heat capacity is constant with respect to the number of deuterium in the cluster, i.e. a light water cluster shows little or no difference in heat capacity from a heavy water cluster. As a comparison, the heat capacity of liquid heavy water in bulk and at room temperature has been measured to be 13% higher than the heat capacity of of light water [18].

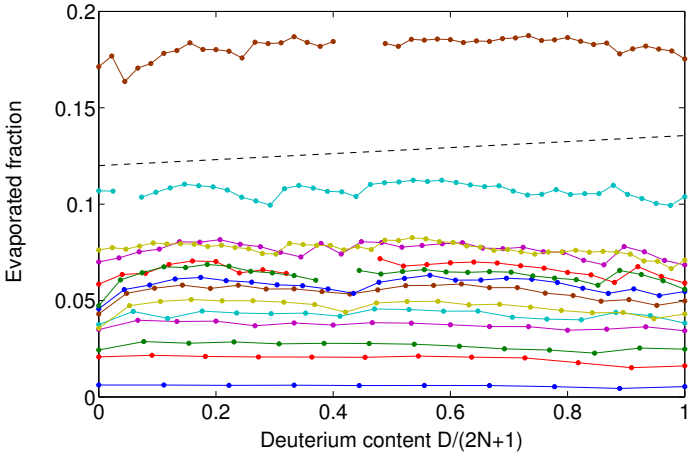

Figure 4.5: Total metastable decay fraction as a function of the relative deuterium content for all cluster sizes decreasing from top to bottom. Colors correspond to the cluster sizes as in figure 4.4. The dashed line is a the expected increase in evaporation from bulk water because of the higher heat capacity of bulk D_2O.

The observation of similar heat capacities also relates to the level densities of the clusters. The level density of a cluster can be expressed using the entropy in the following way [6],

$$\rho(E) \approx \frac{1}{2\sqrt{C_v}T} e^{S(T)}, \tag{4.8}$$

where the canonical entropy $S(T)$ is defined as

$$S(T) = \int_0^T \frac{dE}{T'} = \int_0^T \frac{C_v dT'}{T'}. \tag{4.9}$$

We can conclude that if the heat capacities C_v are the same irrespective of D, the entropy and level densities will be similar as well, assuming the heat capacities are similar at lower temperatures as well. This approximation is very useful in Section 4.4 when we want to compare level densities of clusters that are similar except for their deuterium content.

4.3 Branching ratios

Branching ratios are a measure of the relative losses through each competing decay channel, defined as,

$$B_d = \frac{I_d}{I_0 + I_1 + I_2}, \tag{4.10}$$

with $d = 0, 1, 2$ corresponding to loss of H_2O, HDO and D_2O respectively. B_0, B_1 and B_2 is plotted for N = 4 in Figure 4.6.

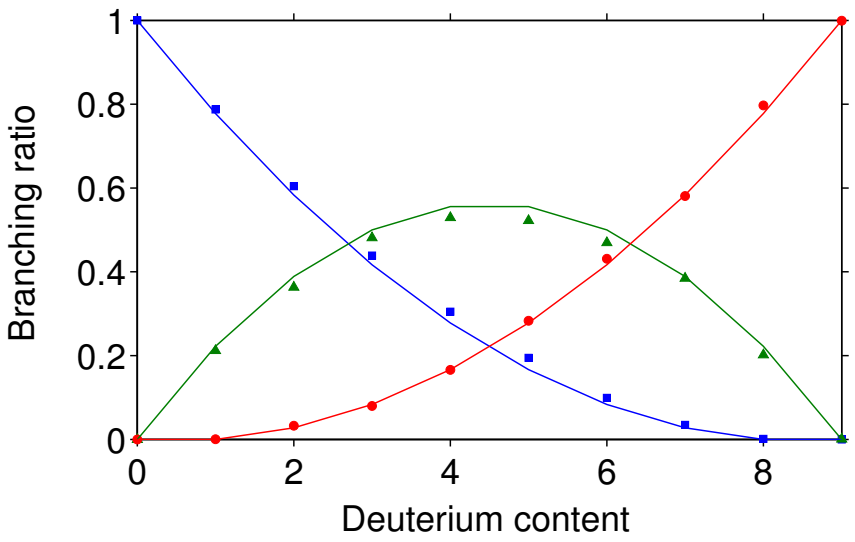

Figure 4.6: Branching ratios of H_2O (squares), HDO (triangles) and D_2O (circles), for cluster size N = 4. The lines are the populations of the different isotopes as described in the text.

The asymmetry towards higher H_2O evaporation is apparent in all cluster sizes from $N = 5$ and larger. If we plot the branching ratios as a function of relative deuterium content $D/(2N + 1)$ we find that all clusters $N = 9$ and larger scale. This is plotted in Figure 4.7.

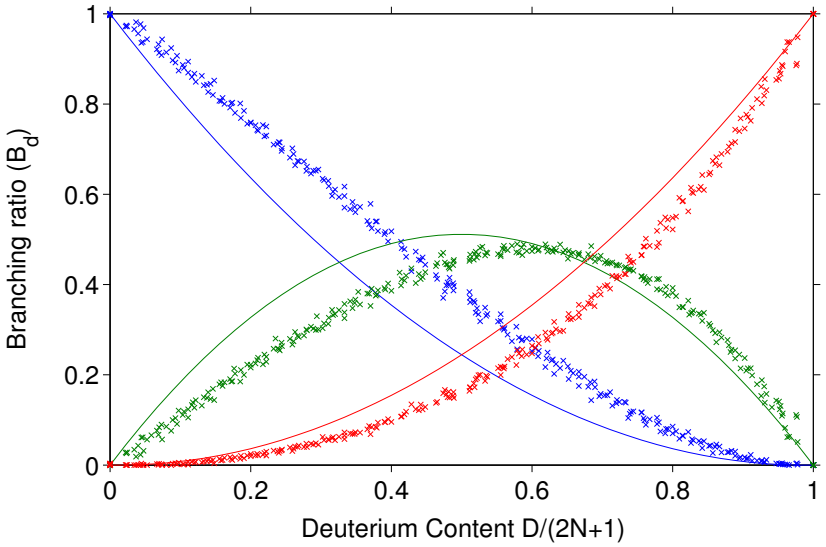

Figure 4.7: Branching ratios of H_2O (blue), HDO (green) and D_2O (red), for cluster sizes N = 9 - 14 and N = 20-22, plotted as a function of the relative deuterium content in the cluster $D/(2N+1)$. The lines are the populations of the different isotopes as described in the text.

The branching depends on the decay rates as well as the population of $d = 0, 1, 2$ in the cluster. Assuming full statistical mixing (scrambling) of H number of hydrogen and D deuterium (with $H + D = 2N + 1$), the relative population of each isotopologue in the cluster is given by [19]

$$P_0 = \frac{H}{H+D}\frac{H-1}{H+D-1}, \tag{4.11}$$

$$P_1 = 2\frac{H}{H+D}\frac{D}{H+D-1}, \tag{4.12}$$

$$P_2 = \frac{D}{H+D}\frac{D-1}{H+D-1}. \tag{4.13}$$

They are obtained by counting the number of different ways in which one can fill the two sites of a water molecule with $d = 0, 1, 2$, from a cluster of H hydrogen and D deuterium. The populations are plotted as solid lines in figure 4.6 and 4.7. If the rate constants were identical and the distribution of deuterium completely random in the cluster we would expect B_d to equal P_d. The fact that B_d and P_d is observed to be nearly identical in figure 4.6 is a good indication that the cluster does not significantly discriminate the deuterium to a certain configuration. For the larger clusters plotted in Figure 4.7 there is a clear deviation from the populations, indicating isotope effects.

As a measure of the asymmetry towards more H_2O evaporation we can take the difference between the observed branching ratios and the populations P_0, P_1 and P_2. This is plotted as a function of cluster size in figure 4.8, where we can see that the branching ratios are increasingly favored towards loss of H_2O with cluster size. This tendency stabilizes at around $N = 11$ after which the difference between the populations and branching remains constant.

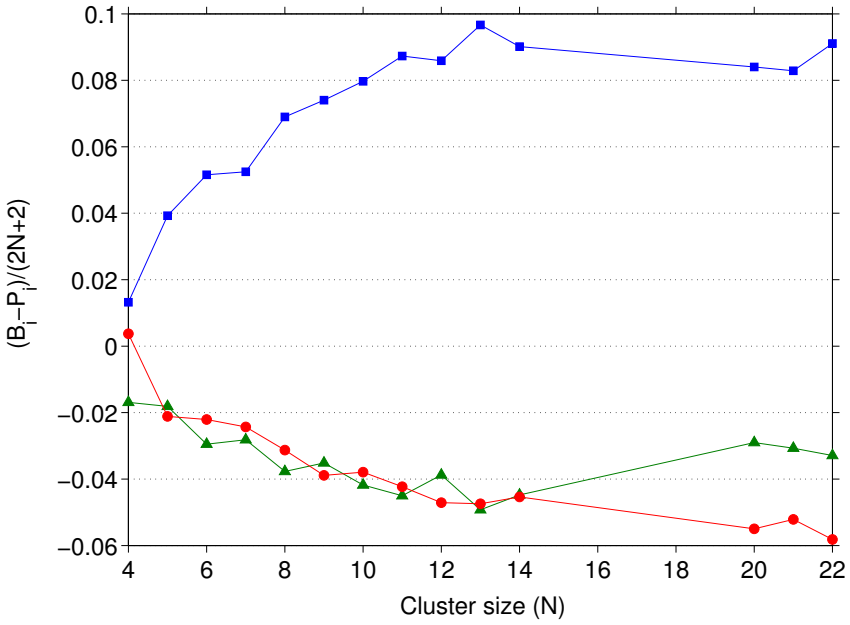

Figure 4.8: Average difference between experimental branching ratios and the populations of each isotope in the clusters as a function of cluster size. Squares are for H_2O, Triangles indicate HDO and circles are D_2O.

4.4 Relative rate constants

This section will expand the analysis of the branching ratios from the previous section in order to observe the true isotope differences without the influence that the populations P_0, P_1 and P_2 have. The number of decayed molecules of each isotopologue has several contributing factors,

$$f_d = k_d P_d \Delta\tau I'_p t \phi \tag{4.14}$$

where $\Delta\tau$ is the time from mass selection (quadrupole) to detection (TOF), I'_p is the parent cluster intensity in s^{-1}, t is the accumulation time of the spectrum and ϕ is the detection efficiency. Here we are interested in the relative decay rate constants k_d.

The probabilities P_0, P_1 and P_2 are divided out of the branching ratios so that we can compare the rate constants $k_d \propto B_d/P_d$ directly. Since the four last factors of equation 4.14 are identical for different d they will cancel out and the relative rate constants are given by $k_d/k_{d'} = (B_d/P_d)/(B_{d'}/P_{d'})$. Note that k_d describes a rate constant under a somewhat constructed cluster scenario that is independent of the number of deuterium in the cluster. These rate constants correspond to what they would be if the entire cluster was of the evaporated species. Even though these are not physical rate constants they are easily compared with each other and the derived expression for the rate constant in Eq. (2.17), and therefore serve their purpose well. The ratio of B_d to $B_{d'} \cdot (P_d/P_{d'})$ is plotted in fig 4.9.

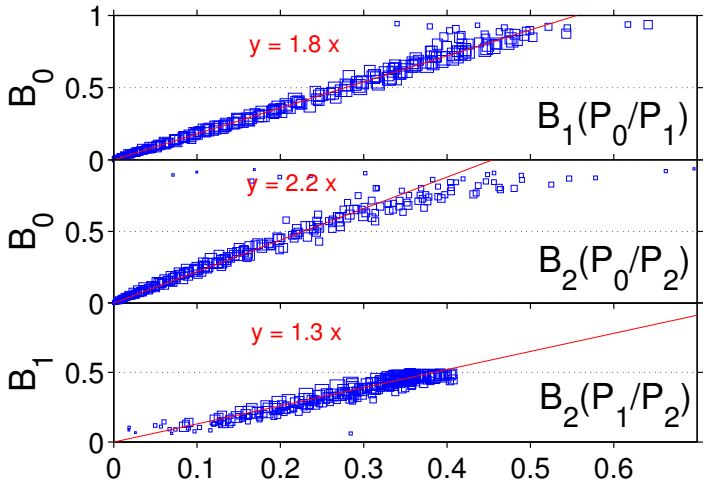

Figure 4.9: Comparison of branching ratios for cluster size N = 9 and larger, with the relative populations divided out. The area of the markers are inversely proportional to one standard deviation. The slope represents the average ratio of decay rates $k_d/k_{d'}$.

All the plotted curves for $N = 9$ and larger is seen to overlap nicely and the average ratio of rate constants are found here as the slope with $k_0 : k_1 : k_2 := 1 : \frac{1}{1.8} : \frac{1}{2.2} = 1 : 0.55 : 0.43$. This means that light water decays from clusters with more than twice the rate of heavy water, with the rate constant of HDO in between. The fact that all cluster sizes larger than $N = 9$ fall on the same line is remarkable but in accordance with figure 4.7 and 4.8 where the asymmetry evens out at around $N = 10$.

We can relate the observed ratio of rate constants to a difference in dissociation energies of the isotopes by taking the ratio of the derived expression for the rate constant from eq. (2.17).

$$\frac{k_d}{k_{d'}} = \frac{\mu_d}{\mu_{d'}} \frac{\sigma_d(E)}{\sigma_{d'}(E)} \frac{Z_d(T_d)}{Z_{d'}(T_d)} \left(\frac{T_d}{T_{d'}}\right)^2 \frac{\rho_d(E - E_{a,d})}{\rho_{d'}(E - E_{a,d'})} \tag{4.15}$$

If the ratio of level densities had the same energy argument, we could now use the observation of section 4.2 and assume the level densities to be the similar since they only differ one deuterium from each other. The level density is, however, a strongly varying function of energy so even a small difference in the dissociation energies $\Delta E_{d,d'} = E_{d'} - E_d$ is not negligible. Assuming the difference in dissociation energies $\Delta E_{d,d'}$ is small compared to the internal energy of the daughter cluster $E - E_{a,d}$ we can expand the logarithm of $\rho_{d'}(E - E_{a,d'})$ around $E - E_{a,d}$,

$$\rho_{d'}(E - E_{d'}) = \rho_{d'}(E - (E_d + \Delta E_{d,d'})) \tag{4.16}$$

$$\approx \rho_{d'}(E - E_d)e^{-\Delta E_{d,d'}/k_B T}. \tag{4.17}$$

This first order approximation allows us to evaluate the level densities in eq. (4.15) at the same internal energy and we can set the ratio to unity. In this approximation the relative rate constants are reduced to,

$$\frac{k_d}{k_{d'}} = \frac{\mu_d}{\mu_{d'}} \frac{Z_d(T_d)}{Z_{d'}(T_{d'})} \left(\frac{T_d}{T_{d'} - \Delta E_{d,d'}/C_v} \right)^2 e^{-\Delta E_{d,d'}/k_B T_d} \tag{4.18}$$

The ratio of partition functions was calculated in section 2.2 and the ratio of reduced masses $\mu_0 : \mu_1 : \mu_2$ is close to $0.9 : 0.95 : 1$. Further, we will assume the ratio of attachment cross-sections $\sigma(E)$ to be unity. By using the calculated maximum daughter temperature from section 2.2 we can relate the observed ratios of rate constants to the difference in dissociation energies for the different isotopologues. With a daughter temperature of $T_0 \approx 140K$ for $N =$ 9- 22 and the ratio of partition functions of $Z_0 : Z_1 : Z_2$ of $1 : 4.9 : 5.8$ we find the difference in dissociation energies to be $\Delta E_{0,1} \approx 25.8$meV, $\Delta E_{0,2} \approx 31.0$meV and $\Delta E_{1,2} \approx 6.4$meV. These values reflect the average number of hydrogen bonds and the relative strengths of the H and D bond, which is discussed further in Chapter 5.

We now move on to establish the relative rate constants for the smaller clusters as well. The average $k_d/k_{d'} = (B_d/P_d)/(B_{d'}/P_{d'})$ vs. cluster size N is plotted in figure 4.10. The ratio of decay rates is seen to increase up to N = 11, after which they converge to the average value of $k_0 : k_1 : k_2 := 1 : 0.56 : 0.43$ as observed previously. Figure 4.10 represents one of the main results of this thesis, where we have extracted the relative rate constants of light and heavy water as a function of cluster size. The rest of this section will be devoted to explaining the difference, using the derived expression for the rate constant eq. (2.17).

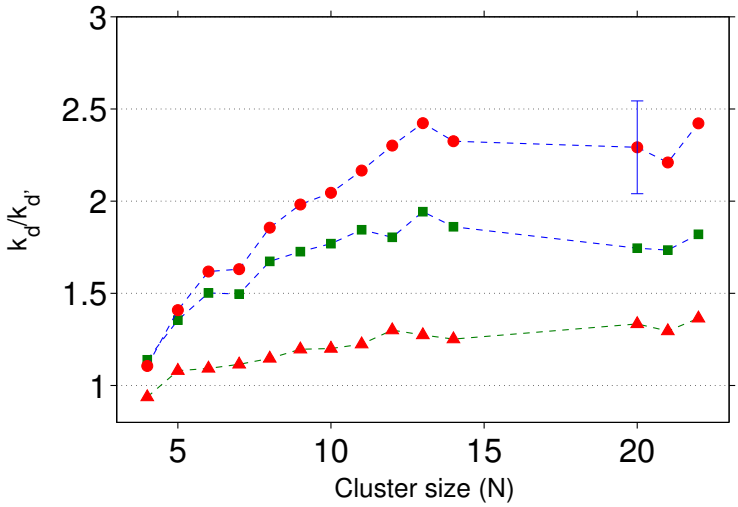

Figure 4.10: Relative decay rates averaged over D for each cluster size. Circles correspond to k_0/k_2, squares k_0/k_1 and triangles k_1/k_2. The error-bar represents a typical root mean square deviation of the data points that were averaged over. The largest deviation was for k_0/k_2 which is plotted at the 1σ level.

We will now treat these relative rate constants in the same manner as in eq. 4.18 to see how the dissociation energies changes with cluster size. The temperatures and partition-functions in table 2.3 are used along with Eq. (4.18) to find $\Delta E_{d,d'}$. The extracted difference in dissociation energies $\Delta E_{d,d'}$ is shown by cluster size in figure 4.11.

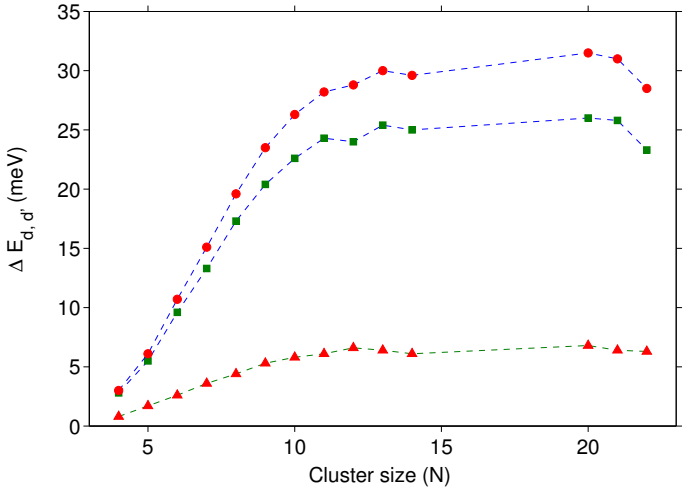

Figure 4.11: Difference in dissociation energies vs. cluster size. Circles correspond to $E_2 - E_0$, squares $E_1 - E_0$ and triangles $E_2 - E_1$.

The difference in dissociation energies increases almost linearly with size and flattens out around $N = 12$. This observed size dependence tells us something about the structure of the clusters. On average one expects more hydrogen bonds per molecule with increasing cluster size, up to the point where adding another molecule does not significantly change the number of bonds and structure. The extracted energies represent another main result of this thesis since they are useful in of themselves and they relate to both isotope effects and hydrogen bonds.The observed difference will be compared with previous experiments and calculations of the difference in bond-strength between H and D bonding in Chapter 5.

4.5 Rate constants vs. D

In the previous section we assigned the ratio of rate constants partly to a difference in energy of the hydrogen and deuterium bond. Apart from the bonds that need to be broken between hydrogen in the evaporating molecule and oxygen in the cluster (henceforth *d*-bonds), we also expect hydrogen isotopes in the cluster to bond with the oxygen in the molecule (henceforth *O*-bonds). In this manner we expect the rate constants to be affected by the number of deuterium in the cluster.

We can find out how the rate constants depend on D, by using the branching ratios and Eq. (4.14) and (4.7) as,

$$B_d/P_d = \frac{I_d}{I_0 + I_1 + I_2}\frac{1}{P_d} = \frac{k_d P_d \Delta\tau I'_p t\phi}{I'_p t(f_m/(1-fm))}\frac{1}{P_d} \tag{4.19}$$

$$= \frac{k_d \Delta\tau\phi}{(f_m/(1-fm))} = c \cdot k_d, \tag{4.20}$$

where c is a constant. We have used the results of section 4.2.2 that the metastable decay fraction f_m does not depend on D. It is also assumed that $\Delta\tau\phi$ does not significantly depend on D and are similar for $d = 0$, 1 and 2. $B_d/(P_d Z_d \mu_d)$ is plotted in fig 4.12 for clusters larger or equal to $N = 10$.

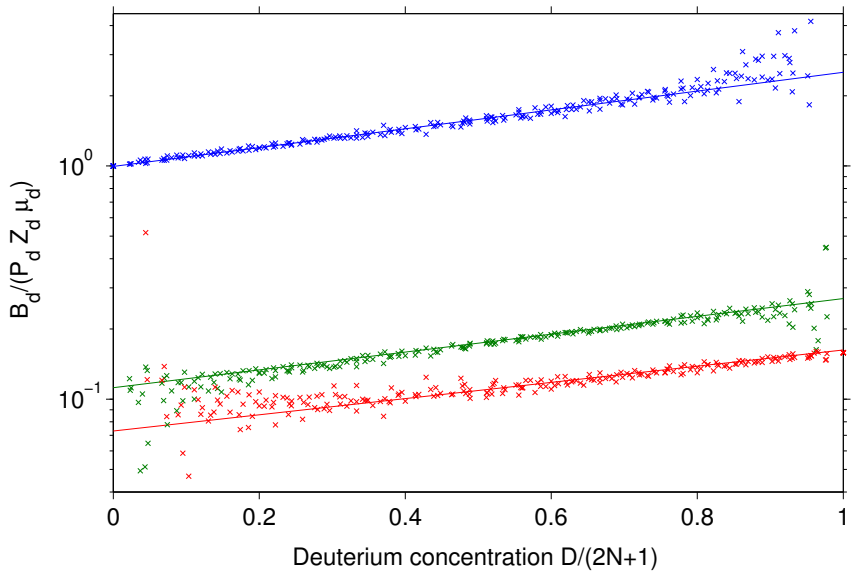

Figure 4.12: Branching ratios with the populations P_d and partition-functions Z_d divided out as a function of relative deuterium content D. $d = 0, 1, 2$ from top to bottom. These are directly proportional to the rate constants k_d. Lines are exponential fits to the decay rates vs. deuterium content. Exponential coefficients are 0.93, 0.88 and 0.80 for $d = 0, 1, 2$.

The rate constant is exponential in the deuterium concentration in the cluster, $D/(2N+1)$, with slightly different exponential factors. The internal partition-functions Z_d of the evaporated water molecules as well as the reduced mass μ_d have been divided out so that the D-dependence reflects only the ratio of daughter- to parent- level-density,

$$B_d/(P_d Z_d \mu_d) \propto \frac{\rho_{N-1,D-d}(E - E^a_{N,D,d})}{\rho_{N,D}(E)}. \tag{4.21}$$

The daughter temperature and cross-section are assumed not to depend on D or d and therefore do not give rise to the observed exponentials. We can try to reconstruct the observed dependence by modeling the factors that contribute to the dissociation energy. Based on the simplest model that accounts for the difference in hydrogen bond energies of hydrogen and deuterium we can express the total energy in the parent and daughter cluster as,

$$E_{N,D} = E_N + \Delta E \cdot D, \tag{4.22}$$

$$E_{N-1,D} = E_{N-1} + \Delta E \cdot D, \tag{4.23}$$

where ΔE is the difference in energy per deuterium added to the cluster. The dissociation energies $E^a_{N,D,d}$ for losing $d = 0, 1$ and 2 are in this case simply the difference in energy between parent and daughter cluster,

$$E^a_{N,D,d} = E_{N,D} - E_{N-1,D-d} = E^a_{N,D,0} + d \cdot \Delta E. \tag{4.24}$$

Since we are interested in the exponential dependence and not the absolute values, we can relax the assumption that ΔE is linear in d, and just use the obtained values of $\Delta E_{d,d'}$ from the previous section. This means relaxing the condition that changing two hydrogen bonds for deuterium has exactly twice the effect of changing one. This model does not yet explain the observed exponential D-dependence and second order effects will have to be included.

The model is modified to introduce an interaction between the deuterium D in the environment and the d-bonds between the evaporated molecule and the rest of the cluster,

$$E^a_{N,D,d} = E^a_{N,D,0} + \Delta E_{d,d'} + \gamma \frac{D-d}{2N-1}. \tag{4.25}$$

Here γ is the change in dissociation energy of the d-bonds in case all the hydrogen around the evaporated molecule are substituted for deuterium. The probability that the deuterium interacts with the evaporated molecule is just the deuterium concentration $(D-d)/(2N-1)$. Similarly the deuterium d in the molecule will have an effect on the O-bond energy and this term is also added to yield,

$$E^a_{N,D,d} = E^a_{N,0,0} + \Delta E_{d,d'} + \gamma \frac{D-d}{2N-1} + d \cdot \xi \frac{D-d}{2N-1}. \tag{4.26}$$

ξ is the change in O-bond energy for every deuterium d in the evaporated molecule. This model is used to relate the observed exponentials to interactions between deuterium in the cluster and deuterium in the evaporated molecule. These second order interactions could be caused by the change of vibrations, electron configurations, symmetries and other effects on the bonds when substituting hydrogen with deuterium.

The daughter level density in Eq. (4.21) is expanded around $E - E^a_{N,0,0}$ such that,

$$k_d \propto \frac{\rho_{N-1}(E - E^a_{N,0,0})}{\rho_{N,D}(E)} e^{\frac{1}{k_B T}\left(-\Delta E_{d,d'} - \gamma \frac{D-d}{2N-1} - d \cdot \xi \frac{D-d}{2N-1}\right)}, \tag{4.27}$$

which can be directly related to the observed exponentials. With $d = 0$ we are seeing only the γ term of k_0 and the observed slope in figure 4.12 is $\gamma = -0.93\ k_B T$ or $\gamma \approx 11.5$ meV. This γ is used to find ξ from the slopes of k_1 and k_2 to be $\xi = 0.08 k_B T \approx 0.97$ meV. By dividing out the exponential factors that depend on d from k_0, k_1 and k_2, i.e. $\Delta E_{d,d'}$ and the ξ term, all the points should fall on the same curve. This is plotted in figure 4.13.

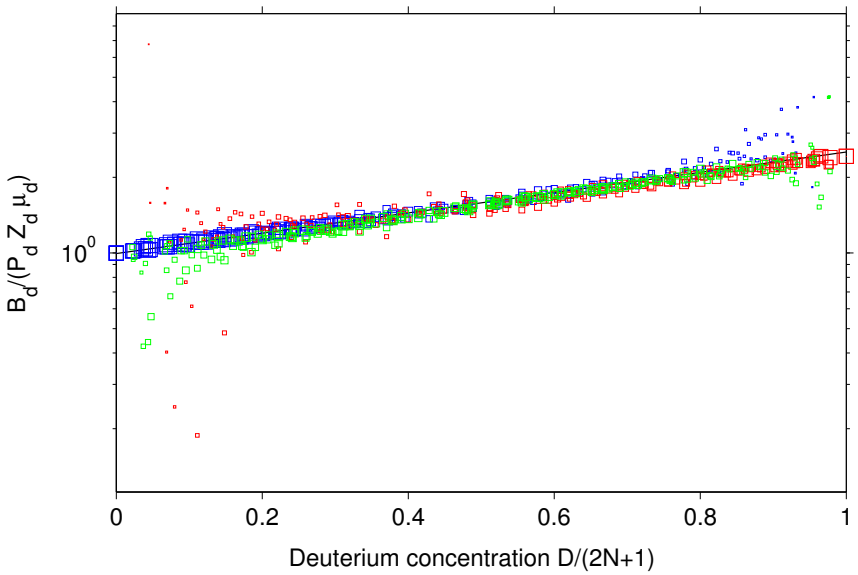

Figure 4.13: Branching ratios with $P_d Z_d \mu_d$ and $\exp\left(-\Delta E_{d,d'} - d\xi(D-d)/(2N+1)\right)$ divided out as described in the text with $\xi = 1$ meV. These are plotted as a function of the deuterium concentration in the cluster. Blue, Green and Red points correspond to $d = 0, 1, 2$ respectively.Area of the symbols are inversely proportional to one standard deviation.

If this model is an accurate representation of the physical mechanism behind the exponential D dependence, we have learned that although the deuterium bond is stronger than the hydrogen bond, this effect is weakened by the second order interactions. A molecule sitting in a deuterium-only environment before evaporating will have 12 meV lower dissociation energy from 'indirect effects' compared to the hydrogen only environment. This effect is altered in the opposite direction when instead adding deuterium to the molecule that evaporates. Each deuterium addition to the evaporated molecule decreases the interaction γ-effect by 8% and again leads to an increase in dissociation energy. These opposite γ- and ξ-effects are not yet understood. It is unclear whether the observed effects are indeed because of a difference in dissociation energies or rather a change in the level density itself with added D. Even if it is the energy it is not unlikely that this model is too simplistic to accurately represent such a complex system. This will be discussed further in the next chapter.

5

Discussion and conclusions

An expression was derived in Chapter 2 for the statistical decay of water molecules from a cluster, Eq. (2.17). In this expression there are several potential causes of the observed difference between the rate constants of light and heavy water. One of these that was only briefly mentioned is the cross-section σ. Since we are dealing with polar molecules and ionic clusters it is not at all certain that σ is geometrical in nature, as was assumed in Section 2.2. The temperature calculation is, however, insensitive to the exact form of σ, and the approximation is valid. In taking the ratio of rate constants we have also ignored the difference in cross-sections between H_2O, HDO and D_2O. If the geometrical cross-section is used, we know D_2O to be slightly smaller because the heavier mass of deuterium leads to a more localized vibrational displacement about the equilibrium position. Compared to the dissociation energies which enter exponentially in the level-density and the ratio of partition-functions this difference is still negligible.

It is interesting to note that the partition functions and in particular the spin statistical degeneracies increases the evaporation of D_2O and HDO almost a factor 6 and 5 respectively, since they have more final states to decay to. This is contested by the different dissociation energies to favor H_2O decay in the end. Thus we have competing effects in the evaporation between the partition functions and the stronger hydrogen-bonds of deuterium.

The relative rate-constants of water isotopologues was measured under near identical conditions in vacuum. The rate-constants are very similar to each other at $N = 4$ and branch off towards more H_2O decay with increasing cluster size. This tendency stops at $N = 12$ where the ratio remains constant, with $k_{H_2O} : k_{HDO} : k_{D_2O}$ close to $1 : 0.56 : 0.43$. As a comparison a study of ice-layers in bulk reported the desorption of H_2O to be favored by a factor 2.2 compared to D_2O [4]. The observed difference was

ascribed to a difference in the principal moments of inertia and the measured difference in dissociation energies of 39meV. This is consistent with the findings of this thesis which found the difference to be 32 meV in clusters $N = 9$ and larger. This indicates that the larger clusters are ice-like in the structure of their bonds. The observed size-dependence can be attributed to an increase in the average number of hydrogen-bonds. The quantitative analysis of the number of bonds and comparison with structure-calculations of water-clusters is outside the scope of this thesis. A study of isotope effects in evaporation from water-ammonia clusters $NH_4^+(H_2O)_3$ concluded that the relative rate constants for evaporation of H_2O, HDO and D_2O was close to $1 : 0.71 : 0.56$ [20]. A comparison with Figure 4.10 shows this ratio to correspond to the what we observe in cluster size $N = 5 - 7$ in pure water clusters.

Some of the simplifications that was made to arrive at the dissociation energies, may be too optimistic for the smallest clusters. More specifically, the rate-constant and temperature estimates are based on the evaporated fragment being small compared to the cluster. It is therefore important to stress the large systematic uncertainty in the dissociation energies of the smallest clusters. It is possible to expand the level densities to second order to better account for the smallest clusters where E_a may be a significant part of the internal energy of the cluster. A finite heat-bath correction to the temperature can also be employed to further improve the analysis. By modeling the explicit form of the level density, $\rho(E)$, of clusters with different deuterium content it would be possible to better determine the difference in dissociation energies, without having to rely on the assumption that they are independent of D.

We have seen in Section 4.5 that the difference in dissociation energies is not simply a question of adding energies of individual bonds, but may include collective effects and interactions between bonds as well. In some sense this is reassuring, because the observed $\Delta E_{d,d'}$ are not linear in the deuterium content of the evaporated molecule,d, but it also introduces an uncertainty in what $\Delta E_{d,d'}$ correspond to physically. These can not be taken strictly to be the difference in in bonding energy, but should instead be regarded as an 'effective energy' which may have several non-trivial contributions.

A difference of 7.4 meV was measured between a single hydrogen and deuterium-bond for the water dimer in a Kr matrix [21]. Another study comparing hydrogen and deuterium bonds between water and an Iodide anion measured the competing inter- and intra- molecular effects to yield a difference of 6.9 meV in total [22]. Many studies have also been devoted to calculating the expected difference and usually fall between 8 - 13 meV per deuterium bond [23] [24]. These can be compared with the difference between HDO and D_2O from this thesis of $\Delta E_{1,2} = 6.4$ meV, but it is unclear exactly how they are related. Reference [23] also calculated the difference in bonding energy if the bonding hydrogen isotope is ionic and found the effect to be reversed, with ionic hydrogen binding 17.3 meV stronger than ionic deuterium which also applies to the current experiment.

Through this seemingly simple experiment we were able to show that the heat capacity of water clusters is not significantly altered by the number of deuterium in the cluster. The relative rate constants were extracted for all clusters which show a smooth size dependence and a significantly higher rate of losing the light water species compared to the heavier. Using calculations and derived expressions the rate constants were explained in terms of the partition function and different dissociation energies for water isotopologues. We also found the rate constants to increase exponentially with the deuterium concentration in the clusters. This led to the possible observation of some interesting second order interaction effects though the simple model developed.

Before publication of an article the following things should be addressed to make the analysis more rigorous.

- Approximation of the cluster temperatures should include higher order terms and the finite heat bath correction. Expansions of level densities should also include higher order terms to correctly describe the smallest clusters as previously discussed.
- Some underlying assumptions should be investigated further, such as the different cross sections, the assumption of complete scrambling used for finding the populations and the assumption that level densities do not depend on the number of deuterium.
- A more advanced model of the dissociation energy can be developed to understand the physical nature of ΔE, γ and ξ.

Bibliography

[1] J. D. Vieira et. al. *Nature*, Vol. 495:p. 344–347, 2013.

[2] Erika Sundén. Thermal properties of clusters and molecules, phd thesis, 2012.

[3] G. Romanelli et al. *The Journal of Physical Chemistry Letters*, Vol. 4:p. 3251–3256, 2013.

[4] Jamison A. Smith, Frank E. Livingston, and Steven M. George. *Journal of Physical Chemistry B*, Vol. 107:p. 3871–3877, 2003.

[5] Yoshihisa Harada et. al. *Physical Review Letters*, Vol. 111:p. 193001, 2013.

[6] Klavs Hansen. *Statistical Physics of Nanoparticles in the Gas Phase*. Springer, 2013.

[7] V. Weisskopf. *Physical Review*, Vol. 52:p. 295, 1937.

[8] Terry Beyer and D.F. Swinehart. *Communications of the ACM*, Vol. 16(6), 1973.

[9] D. Eisenberg and W. Kauzmann. *The structure and properties of water*. University Press, London, 1969.

[10] Tennyson et al. *J. Phys. Chem. Ref. Data*, Vol 30(3), 2001.

[11] Iupac database of water, http://chaos.chem.elte.hu/marvel/.

[12] G. Mellau et al. *Journal of Molecular Spectroscopy*, Vol. 224:p. 32–60, 2004.

[13] A. E. K. Sundén, K. Støchkel, S. Panja, U. Kadhane, P. Hvelplund, S. Brøndsted Nielsen, H. Zettergren, B. Dynefors, and K. Hansen. *The Journal of Chemical Physics*, Vol. 130, 2009.

[14] Carl W. Kammeyer and Donald R. Whitman. *Journal of Chemical Physics*, Vol. 56(9), 1972.

[15] Mauritz Johan Ryding. Experimental studies of cluster ions containing water, ammonia, pyridine and bisulphate, phd thesis, 2011.

[16] JB Fenn, M mann, CK Meng ans SF Wong, and CM Whitehous. *Science*, Vol. 246(4926).

[17] K. Hansen, P. U. Andersson, and E. Uggerud. *The Journal of Chemical Physics*, Vol. 131, 2009.

[18] Motoyuki Shiga and Wataru Shinoda. *Journal of Chemical Physics*, Vol. 123:p. 134502, 2005.

[19] Klavs Hansen. Private communication, 2013.

[20] A. E. K. Sundén, K. Støchel, P. Hvelplund, S. Brøndsted Nielsen, B. Dynefors, and K. Hansen. Relative light and heavy water evaporation rates from $nh_4^+(h_2o)_3$ clusters. *Not yet published*, 2012.

[21] A. Engdahl and B. Nelander. *Journal of Chemical Physics*, Vol. 86:p. 1819, 1987.

[22] E. G. Diken, JW. Shin, E. A. Price, and M. A. Johnson. *Chemical Physics Letters*, Vol. 387:p. 17–22, 2004.

[23] Steve Scheiner and Martin Cuma. *Journal of the American Chemical Society*, Vol. 118:p. 1511–1521, 1996.

[24] Yoko Kikuta, Takayoshi Ishimoto, and Umpei Nagashima. *Chemical Physics*, Vol. 354:p. 218–224, 2008.